Pattern and Gain Characterization Using Nonintrusive Very-Near-Field Electro-Optical Measurements Over Arbitrary Closed Surfaces

Kamal Sarabandi, *Fellow, IEEE,* Jihun Choi, *Student Member, IEEE,* Ali Sabet, and Kazem Sabet, *Senior Member, IEEE*

***Abstract*— A nonintrusive near-field measurement technique for 3-D radiation pattern and gain characterization of antennas is presented. The method is of particular interest for low-frequency antennas for which anechoic chambers cannot be developed and far-field measurements are rather cumbersome. Nonintrusive, broadband measurements are performed using an extremely small all-dielectric electro-optical probe to measure the tangential electric fields of an antenna under test (AUT) at a very-near surface enclosing the antenna. Far-field radiation is computed from a new near-field to far-field transformation formulation using only the tangential components of the electric field over an arbitrary surface. This procedure employs reciprocity theorem and the excited electric current on the surface of a perfect electric conductor enclosure having the same geometry as the scanned surface and illuminated by a plane wave. In this way, a full spherical radiation pattern and gain of the AUT are easily computed without expensive computation and truncation errors. To demonstrate the proposed approach, a miniaturized low very high frequency antenna operating at 40 MHz with dimensions $0.013\lambda_0 \times 0.013\lambda_0 \times 0.02\lambda_0$ is utilized. The far-field results from our approach are shown to be in good agreement with those obtained from full-wave simulation and direct far-field measurement performed in an elevated outdoor range.**

***Index Terms*— Antenna measurements, antenna radiation patterns, electrically small antennas, electro-optical (EO) system, high frequency (HF)/very HF (VHF) antennas, near-field measurements.**

I. Introduction

ACCURATE measurement of fundamental antenna parameters, such as input impedance, bandwidth, radiation pattern, and gain is very important for all applications. Knowledge of the actual antenna performance plays an important role in designing real-world wireless communication or radar systems. The simplest way to characterize antennas is of course the direct far-field measurement that can be accomplished in outdoor ranges or in anechoic chambers [1]–[3]. The use of such techniques with low-frequency antennas operating at high frequency (HF) or low very HF (VHF) bands is limited by a number of factors. At these frequencies, the sizes of anechoic chambers and the absorbers become prohibitively large. Outdoor ranges require a vast space and tall towers, and the effect of ground must be carefully examined for accurate measurements. Special approaches to measure HF and VHF antennas have been reported in [4]–[9]. These involve scale modeling, utilization of aircraft-towed transmitters in antenna measurements, design of ground-reflection ranges to minimize the contribution of reflection from the ground, and near-field scanning. All of these require substantial time and effort to perform the measurements as well as a specially designed very-large, expensive anechoic chamber in the case of indoor measurements.

In order to circumvent these difficulties, a nonintrusive near-field measurement system [10] using an all-dielectric and very small electro-optical (EO) probe is presented in this paper. The advantage of the EO probe is that it can be placed very close to the antenna surface where the near field is very strong. For a nonmetallic room that is sufficiently larger than the antenna and for the antenna sufficiently away from obstacles in the room, the use of absorbers is not critical. The criteria for setting object distances from the antenna are established by monitoring the reactive part of the antenna input impedance as antenna height above ground is changed and nearby obstacles are pushed away from the antenna surrounding. Once a stable condition for the reactive part of the input impedance is observed, it is assured that the field distribution over the surface of antenna is dominated by the direct signal. Also at low frequencies, reflection and scattering from dielectric walls and objects are rather low. Hence, the contribution from multipath signal on the probe is significantly smaller than the very strong near field of the antenna. Conventional probes, such as loops, short diploes, or open-ended waveguides, which make use of metallic structures together with their connected transmission lines, can significantly perturb the current distribution on the antenna if they are brought to very close proximity of the antenna. This is particularly the case if the antenna under test (AUT) is electrically small whose dimensions are comparable to those conventional probes. Unlike the conventional metallic probes, the EO probe with a very small tip of less

Manuscript received March 18, 2016; revised November 10, 2016; accepted November 27, 2016. Date of publication December 1, 2016; date of current version February 1, 2017. This work was supported in part by the U.S. Army Research Laboratory through collaborative participation in the Microelectronics Center of Micro Autonomous Systems and Technology Collaborative Technology Alliance, under Contract W911NF and in part by the National Science Foundation through ECE Program, under Award 1101868.

K. Sarabandi and J. Choi are with the Radiation Laboratory, Department of Electrical Engineering and Computer Science, University of Michigan, Ann Arbor, MI 48109-2122 USA (e-mail: saraband@eecs.umich.edu; jihchoi@umich.edu).

A. Sabet and K. Sabet are with EMAG Technologies Inc., Ann Arbor, MI 48108 USA (e-mail: ksabet@emagtech.com; asabet@emagtech.com).

Color versions of one or more of the figures in this paper are available online at http://ieeexplore.ieee.org.

Digital Object Identifier 10.1109/TAP.2016.2633949

than 1 mm^3 connected to very thin fiber optics does not perturb the excited currents on the antenna. The EO probe used here is also very broadband and can be applied for all frequencies of interest up to and beyond millimeter-waveband. Furthermore, the computationally complicated probe compensation process [11], [12] is not required, since the EO probe measurement is nonradiative.

In [13] and [14], near-field to far-field transformation for arbitrary enclosing near-field surfaces has been proposed. These approaches, however, provide only an approximate solution under the assumption that the radii of curvature of the surface at every point are much larger than the wavelength. Similar to our approach, they place a perfect electric conductor (PEC) over the aperture of the antenna with a surface magnetic current proportional to the measured tangential electric field. Then, they apply image theory that is only valid for infinite ground plane to remove the PEC and double the surface magnetic current. This is only a good approximation if the local radii of curvature over the arbitrary surface are very large compared with the wavelength. If cubic surfaces are used, the edges do not satisfy this condition. In fact, there is significant edge current on the PEC, which cannot be ignored. It is noted here that the dimension of the box for the problem at hand is only a fraction of the wavelength and image theory cannot be applied here. In this paper, a novel exact near-field to far-field transformation for all types of antennas without truncation errors regardless of the size of the scanned area is presented. For this approach, only the tangential components of the electric field over an arbitrary closed surface encompassing the AUT are required. The reciprocity theorem in conjunction with the induced surface current excited by a plane wave on a metallic surface in place of the scanned enclosing surface is used. The induced surface electric current density illuminated by an incident plane wave in a desired direction over the metallic surface is calculated using a full-wave numerical simulation. Using the reaction theorem, the radiated field in a desired direction is computed as will be shown later. The validity of this antenna characterization technique is demonstrated, utilizing a recently developed miniaturized folded dipole antenna at low-VHF band [2], [15]. The computed antenna parameters from the proposed technique are compared with those obtained from direct far-field measurement in a special elevated range and full-wave electromagnetic (EM) simulation. In Section II, the EO-based near-field approach is presented. In Section III, a new formulation for near-field to far-field transformation applicable for arbitrary shape scanned surface is provided. Section IV presents the measurement calibration and validation of the proposed approach.

II. Electro-Optical Near-Field Measurement

Nonintrusive, high-resolution, near-field measurement is of interest for number of applications, including RF circuit diagnostics, EMC/EMI testing, and antenna characterization. Despite the existence of many near-field radiation pattern characterization methods, as will be shown here, there are a number of important advantages for nonintrusive and high-resolution near-field sampling that EO measurements can provide [16], [17]. One such advantage pertains to the measurement of antennas at low frequencies. For applications, such as source tracking [18] and reliable communication in complex environments [19], [20], an extremely small and lightweight antenna operating at low-VHF band has been developed. For this antenna, pattern and gain measurements were carried out in an outdoor elevated range with nonmetallic towers. A standard far-field measurement setup, in which both the transmitting and the receiving antennas are mounted on top of a tall fiberglass tower (>12 m), was used to create nearly free-space conditions in the far-field region. For this measurement, considerable efforts are needed because of the cumbersome antenna setup and scanning. The height of AUT above ground must also be chosen to be much larger than the transmit and receive antennas separation to minimize the effect of ground reflection. Uncontrollable environmental conditions, such as rain, wind, and temperature variations, also add to the complexity of the elevated-range measurement. Furthermore, for small antennas, the effect of the feed cables on the antenna impedance and radiation pattern is a major issue and was observed during the measurement. A small, battery-operated source module had to be designed and connected directly to the antenna in the elevated range to avoid the effects of the long cables. The complexity in such measurements necessitates the development of an alternative approach that is more accurate and time- and cost-effective.

Near-field scanning systems are developed as an alternative to the cumbersome outdoor far-field range or costly anechoic chamber facilities. However, conventional near-field scanning systems have substantial disadvantages at low frequencies. These systems are traditionally designed for antennas operating at microwave frequencies and higher with large apertures to circumvent the challenges associated with satisfying the far-field requirement. As alluded to before, the standard probes for near-field systems are small metallic antennas or apertures for picking up the near fields of the AUT. Such metallic probes and the associated transmission lines connected to them cannot be placed very close to the AUT, as they can significantly modify the current distribution on the antenna, and thereby would distort the measured near-field distribution. These probes are also band limited and have a relatively large physical dimension at low frequency. For conventional near-field systems, the minimum distance between the probe and the AUT is the far-field distance of the small probes. This minimum distance oftentimes is larger or comparable to the wavelength. For a short dipole, for example, requiring the ratio of the radiating term to the largest nonradiating term to be larger or equal to 10, the far-field distance is computed to be 1.6 λ. Even if we were to relax the radiating to nonradiating terms ratio to be larger than 3, the minimum distance must still be larger than 0.6 λ. Obviously, for an AUT that operates at low-VHF band or lower, this distance amounts to many meters. In [9], for instance, a spherical near-field system in VHF range in a large rectangular anechoic chamber with pyramidal absorber is introduced. The probing distance in the system is large (2 m) due to the use of conventional metallic probe consisting of two resistively loaded crossed dipoles, each 40 cm in length. For the general near-field antenna

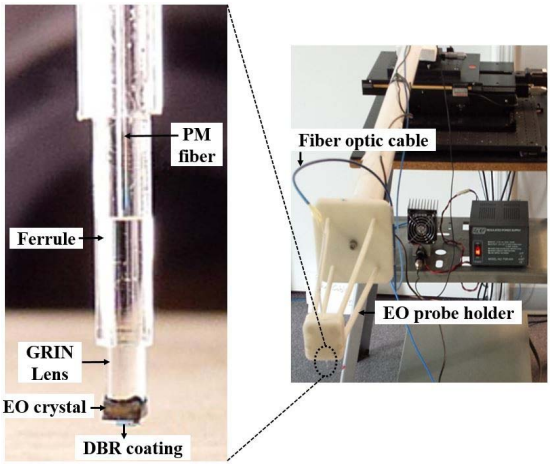

Fig. 1. Fiber-based electro-optic probe structure used in our measurement system.

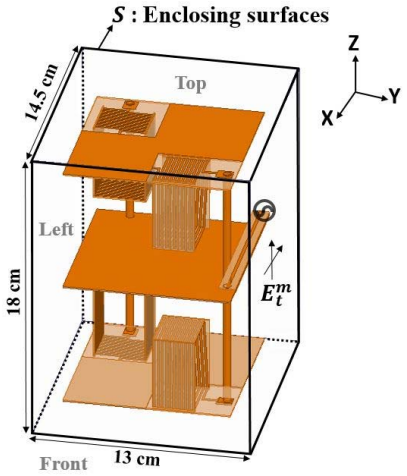

Fig. 2. Imaginary rectangular box composing six scanned surfaces is centered at the origin of a Cartesian coordinate system whose axes are parallel to the edges of the box.

measurement applications of EO probes, in addition to the nonintrusive nature of EO probes, it should be mentioned that probe compensation process is not required [16], [21].

The system employed in this paper is a commercial measurement system, called NeoScan, developed by EMAG Technologies. It provides significantly superior performance to the conventional near-field scanning systems as described before. This system operates based on Pockels effect, which measures the phase retardance of an optical beam through a small crystal immersed within an RF electric field [22]. This EO effect provides a means for modulating the polarization of the optical beam, which makes it possible to detect the presence of an electric field impinging on a very small crystal (1 mm $\times$ 1 mm $\times$ 1 mm) of the EO probe in the system. The EO field probe is all dielectric with no metallic components and can be used to measure the electric fields with extremely small spatial resolution (minimum sampled space <10 μm corresponding to the focused laser beam within the EO crystal). These probes can be brought to the very-near-field region of the antenna where the fields are very strong. Another advantage of the EO probe is an extremely wide bandwidth (3 MHz–100 GHz or higher). The probe can be calibrated to measure the absolute magnitude and relative phase of electric fields over a wide dynamic range (0.1 V/m–1 MV/m). Fig. 1 shows the picture of the EO probe used in our measurements.

III. 3-D Near-Field to Far-Field Transformation

Based on uniqueness theorem, the fields outside a region enclosing the sources of the EM field can be uniquely determined if the tangential electric or magnetic field over the enclosing surface is known. Suppose that the tangential electric field of an AUT over an arbitrary surface enclosing the antenna is measured by the EO probe of NeoScan. Far-field quantities can then be calculated, employing the radiometrically calibrated values of the measured near fields. The geometry of a small antenna enclosed by surface S is shown in Fig. 2. For this problem, the measured tangential electric field is represented by $\boldsymbol{E}_t^m(\boldsymbol{r})$. To calculate the field outside S using just the tangential electric field, the field equivalence principle can be invoked [23]. In this approach, we assume that the fields inside S are zero and introduce instead fictitious surface electric and magnetic currents proportional to the tangential magnetic and electric fields. Since the tangential magnetic field components are not available, the surface S may be replaced by a PEC, over which the surface magnetic current is placed. Thus, the problem is reduced to finding the total field radiated from the magnetic current in the presence of the PEC box having the same surface as S. The magnetic current is given by

$$\boldsymbol{J}_m^m = -\hat{n} \times \boldsymbol{E}_t^m \tag{1}$$

where $\hat{n}$ is a unit vector directed normally outward from S and $\boldsymbol{E}_t^m$ is the electric field generated by the AUT over S.

Of course, for such problems and arbitrary S, an exact analytical solution does not exist. For a rectangular box, for example, one may resort to an approximate analytical solution using image theory. That is, assuming the PEC box consists of electrically large flat sides, the image theory can be applied by doubling the magnetic current on the sides of the enclosing rectangular box and then computing the radiating field in the absence of the box using the planar near-field to far-field transformation [24] for all six surfaces. This approach ignores the truncation effects and can introduce significant error when the dimensions of the box are small or comparable with the wavelength. To resolve this issue, an alternative method based on numerical simulations and the reciprocity theorem is introduced.

Consider the rectangular cuboid as the enclosing surface S centered at the origin of a Cartesian coordinate system whose axes are parallel to the edges of the cuboid. Using the source equivalence principle, the rectangular cuboid surface is made into a PEC surface. Now let us suppose that the metallic cuboid is being illuminated by the fields of an infinitesimal magnetic dipole located at the observation point in the far-field region at a distance r_0 from the origin and at an orientation denoted by θ and ϕ. The volumetric magnetic current distribution for this source can be written as

$$\boldsymbol{J}_m^b = \hat{p}\delta(\boldsymbol{r} - \boldsymbol{r}_0) \tag{2}$$

where $\hat{p}$ is a unit vector along the dipole, r is the radial distance from the origin, and $\delta(\boldsymbol{r}-\boldsymbol{r}_0)$ is a delta function. The far-field expression for the radiated field from the infinitesimal dipole at a point around the origin can be found from

$$\boldsymbol{E}_i^b = \frac{ik}{4\pi}\frac{e^{ikR}}{R}\hat{p}\times\hat{R} \tag{3}$$

where k is the angular wavenumber given by $k = 2\pi/\lambda_0$ and

$$R = |\boldsymbol{r}-\boldsymbol{r}_0| \approx r_0 - \boldsymbol{r}\cdot\hat{r}_0 \tag{4a}$$

$$\hat{R} = \frac{\boldsymbol{r}-\boldsymbol{r}_0}{|\boldsymbol{r}-\boldsymbol{r}_0|} \approx -\hat{r}_0 \tag{4b}$$

$$\hat{r}_0 = \sin\theta\cos\phi\hat{x} + \sin\theta\sin\phi\hat{y} + \cos\theta\hat{z}. \tag{4c}$$

Upon inserting (4a) and (4b) into (3), we have

$$\boldsymbol{E}_i^b = \frac{-ik}{4\pi}\frac{e^{ikr_0}}{r_0}e^{-ik\hat{r}_0\cdot\boldsymbol{r}}\hat{p}\times\hat{r}_0. \tag{5}$$

In a similar manner, it can be shown that

$$\boldsymbol{H}_i^b = \frac{-ik}{4\pi\eta_0}\frac{e^{ikr_0}}{r_0}e^{-ik\hat{r}_0\cdot\boldsymbol{r}}\left(\hat{p}\times\hat{r}_0\right)\times\hat{r}_0 \tag{6}$$

where $\eta_0 = \sqrt{\mu/\varepsilon}$ is the free space characteristic impedance. Applying the reaction theorem [25] to the surface and volumetric magnetic currents given by (3) and (4) leads to

$$\iint_S H^b(r)\cdot J_m^m(r)ds = \iiint H(r)\cdot J_m^b(r)dv \tag{7}$$

where $\boldsymbol{H}^b(\boldsymbol{r})$ is the total magnetic field (incident plus scattered) generated by the infinitesimal magnetic current source on the surface of the enclosing PEC box. Also, $\boldsymbol{H}(\boldsymbol{r})$ is the radiated field from the AUT. Here, we have used the fact that the tangential component of the total electric field $\hat{n}\times\boldsymbol{E}^b(\boldsymbol{r})$ is equal to zero on the surface according to the boundary condition over PEC surfaces, such that the surface integral of its term over the box disappears.

Using (1) and (2) in (7), the radiated magnetic field from the AUT can be calculated from

$$\hat{p}\cdot\boldsymbol{H}(\boldsymbol{r}_0) = -\iint_s \boldsymbol{H}^b(\boldsymbol{r})\cdot\hat{n}\times\boldsymbol{E}^m(\boldsymbol{r})\,d\boldsymbol{s}. \tag{8}$$

Noting that $\hat{n}\times\boldsymbol{H}^b = \boldsymbol{J}_s^b(\boldsymbol{r})$ is the induced electric current on the surface of the PEC enclosure

$$\hat{p}\cdot\boldsymbol{H}(\boldsymbol{r}_0) = \iint_s \boldsymbol{E}_t^m(\boldsymbol{r})\cdot\boldsymbol{J}_s^b(\boldsymbol{r})\,d\boldsymbol{s}. \tag{9}$$

Hence, the radiated magnetic field in the direction of $\boldsymbol{r}_0$ can easily be attained from the measured tangential electric field and the calculated induced surface electric current density over the PEC box. To further simplify calculation of $\boldsymbol{J}_s^b(\boldsymbol{r})$, plane wave excitation instead of the magnetic dipole source may be considered. This can be done, since the infinitesimal magnetic dipole is in the far-field region of the AUT. Accordingly, the incident electric field given by (5) can be locally regarded as a plane wave. Denoting the induced surface current on the PEC enclosure from an incident plane wave with intensity 1 V/m and polarization $\hat{p}\times\hat{r}_0$ propagating along $-\hat{r}_0$ by $\boldsymbol{J}_s^p(\boldsymbol{r})$, (9) can be written as

$$\hat{p}\cdot\boldsymbol{H}(\boldsymbol{r}_0) = \frac{-ik}{4\pi}\frac{e^{ikr_0}}{r_0}\iint_s \boldsymbol{E}_t^m(\boldsymbol{r})\cdot\boldsymbol{J}_s^p(\boldsymbol{r})ds. \tag{10}$$

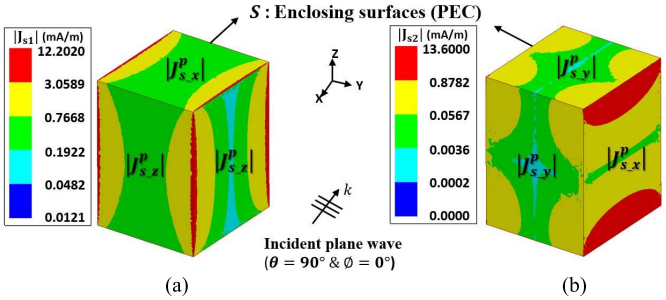

Fig. 3. Magnitudes of the induced surface electric currents on the PEC enclosure S, illuminated by an incident plane wave at a given direction ($\theta = 90°$ and $\emptyset = 0°$).

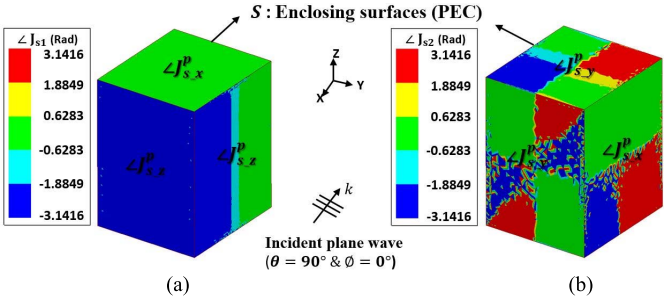

Fig. 4. Phases of the induced surface electric currents on the PEC enclosure S, illuminated by an incident plane wave at a given direction ($\theta = 90°$ and $\emptyset = 0°$).

It is noted that $\boldsymbol{J}_s^p(\boldsymbol{r})$ can be computed analytically for canonical enclosures, such as spheres and cylinders or numerically for the others using a standard full-wave approach. Figs. 3 and 4 show an example of the computed induced surface electric current density over the PEC enclosure in terms of magnitudes and phases when a plane wave with the intensity of 1 V/m at $\theta = 900^{\circ}$ and $\emptyset = 0^{\circ}$ is incident on S. Similarly, by computing all the induced surface currents as a function of θ and ϕ, and then applying them into (10) with the measured very-near fields, the radiated electric field ($\boldsymbol{E} = \eta_0\boldsymbol{H}\times\hat{r}_0$) from the AUT is calculated. Here, numerical calculation of the integrals in (10) is performed based on trapezoidal method of integration [26].

The antenna gain can be computed, since the value of the electric field and the input power P_{in} to the AUT is available. First, the radiation intensity $U(\theta,\emptyset)$, defined as the power radiated from an antenna per unit solid angle, is evaluated from the calculated far field. Defining electric-field intensity $\boldsymbol{E}(r)$ of the AUT at the far-field region as

$$\boldsymbol{E}(r) = \frac{e^{-jkr}}{r}[F_\theta(\theta,\phi)\hat{\theta} + F_\phi(\theta,\phi)\hat{\phi}] \tag{11}$$

where $F_\theta(\theta,\phi)$ and $F_\phi(\theta,\phi)$ are the radiated electric field strength from the AUT in the (θ,ϕ) direction, the antenna gain G can then be expressed as [27]

$$G = \frac{4\pi U(\theta,\emptyset)}{P_{in}} \tag{12}$$

where

$$U(\theta,\emptyset) = \frac{1}{2\eta_0}[|F_\theta(\theta,\phi)|^2 + |F_\phi(\theta,\phi)|^2].$$

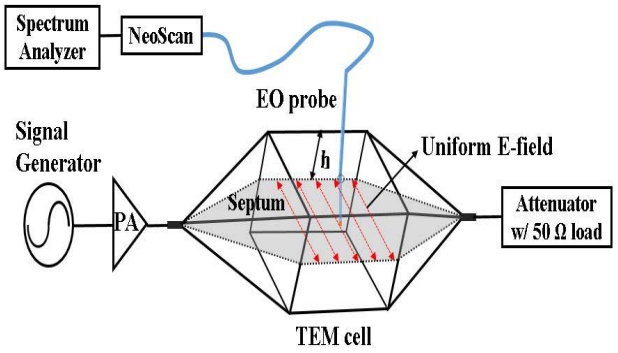

Fig. 5. Experimental schematic of the EO probe calibration system utilizing a standard TEM cell.

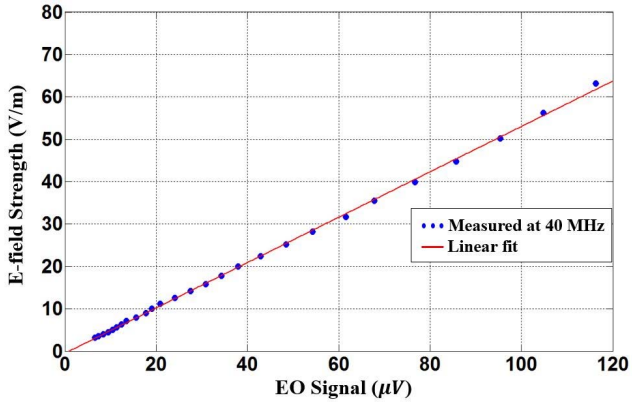

Fig. 6. Actual electric field strength corresponding to its EO signal captured by the EO field probe. This graph shows a linear relationship between them.

IV. Measurement Calibration and Validation

In order to maintain the accuracy and reliability of very-near-field antenna measurements, the field probe system must remain stable over the entire measurement period. Stabilization of the EO probe in our system is consistently monitored by a managing program developed with a system design software (National Instruments LabVIEW 2011) while the probe scans near fields of the AUT. In order to achieve the maximum EO signal at a given condition for the best probe sensitivity, a system optimization procedure is also conducted. This involves determining a stable optimal bias point applied to a polarization controller consisting of four dynamic retardation plates in NeoScan, which is utilized to control a polarization state of the optical beam in the fiber.

The EO system directly measures the intensity of modulated optical beams due to the variation of the RF electric field signals. To obtain the absolute value of the electric field, the probe has to be calibrated against a known field. In other words, the probe calibration is used to find the linear relationship between the measured signal power from the system output and the electric field intensity at the probe tip. This calibration can be performed using a standard transverse EM (TEM) cell in which a known and uniform electric field is established [28], [29]. In the cell, since the field strength is related to the net input power produced by an RF source, the electric field in terms of the input power can be calculated [30]. Thus, the EO probe can be calibrated by sensing the known fields for a certain RF input power. As shown in Fig. 5, in our calibration setting, a uniform electric field is linearly polarized in a direction parallel to the septum in the TEM cell. Therefore, by aligning the axis of the EO crystal at the tip of the probe so as to sense horizontally polarized fields and then by placing the probe in the center of the test region through a small hole in the top wall of the cell, the probe is calibrated for the correct polarization. A power amplifier (PA), which can provide a continuous-wave output power up to 20 W, is utilized to characterize the EO probe over a wide dynamic range. The EO signals measured using a spectrum analyzer versus the calculated electric field strength corresponding to the net power in the cell at 40 MHz (the center frequency of AUT) are presented in Fig. 6. The calibration slope shows a good linear relation between the EO signal in μV and the electric field intensity in V/m.

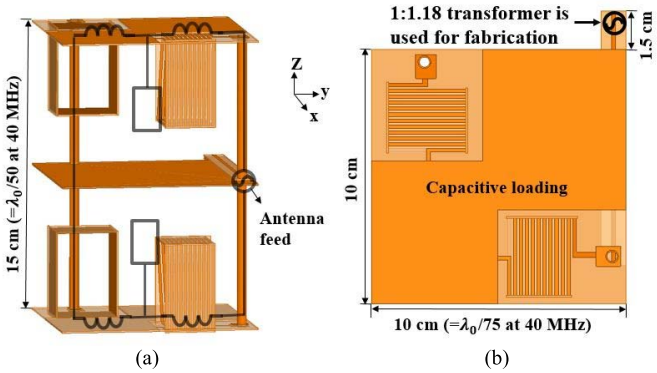

Fig. 7. (a) Side and (b) top view of a VHF miniaturized folded dipole antenna used as the AUT. The circuit model is superimposed on the side view.

This linearity can be denoted by $E = \alpha V$, where α is the calibration coefficient.

A. Test Antenna

To demonstrate the unique capability of the EO-based near-field measurement, a recently developed miniaturized antenna operating near 40 MHz is used as AUT. Antenna miniaturization is realized by introducing 180° phase shifters that are composed of lumped inductors and an open stub, in which both ends of the phase shifters are connected to two short, vertical wires that are radiating in-phase [2], [15]. In this way, in-phase vertically polarized fields at resonance can be produced from the wires, which results in doubling the antenna effective height, and consequently, enhanced gain without physically increasing the antenna height. Moreover, to minimize the overall antenna loss and mass, optimized rectangular air-core inductors with high quality factor (Q) are used in the phase shifters. Fig. 7 shows the side and top view of the antenna with its equivalent circuit model superimposed over the side view. Input reflection coefficient S_{11} of the antenna is simulated by a full wave EM simulator (Ansoft HFSS 15) based on the finite-element method and compared with that of the fabricated one measured with a calibrated network analyzer, as shown in Fig. 8. The resonant frequency of the AUT is measured to be 40.06 MHz, which is in good agreement with the simulation.

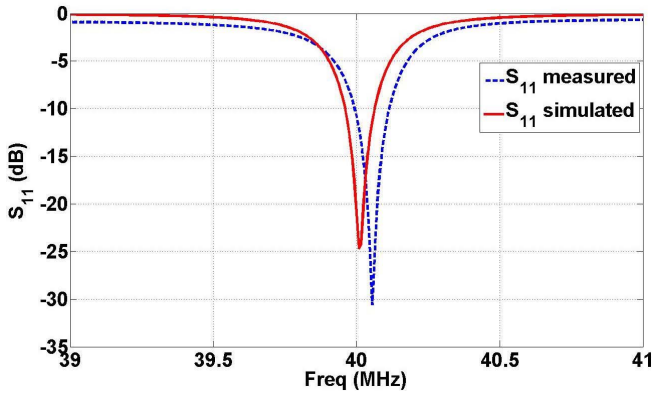

Fig. 8. Measured and simulated input impedance of the designed antenna.

B. Measurement Results

As mentioned earlier, the surface of rectangular cuboid enclosing the AUT is considered as the probed surface. This allows for the utilization of planar near-field scanning that requires a simple X–Y translation unit. The planar near-field scanning is performed over six surfaces of the rectangular cuboid, as shown in Fig. 2. The spatial resolution of the scanned grid and the probe distance from the aperture of the AUT are also important parameters of the measurement setup. According to the sampling theorem [31], the spacing between sampled points must be at least $\lambda_o/2$ so as not to introduce reconstruction errors known as aliasing. Moreover, the spatial resolution is related to probe distance in the sense that choosing one would determine the other. For large aperture antennas, the higher is the sampling interval, the faster and more efficient is the measurement. The common relationship used between the sampling interval and probe distance is given by [24]

$$\Delta s = \frac{\lambda_0}{2\sqrt{1+\left(\frac{\lambda_0}{d_p}\right)^2}} \tag{13}$$

where Δs is the sampling interval and d_p is the probe distance. For small antennas that are proportional or smaller than a wavelength, the sampling interval should be even smaller than what is given by (13). As mentioned before, for small antennas at low frequencies, measurements should be performed very near to the smallest antenna-enclosing surface. This ensures that the dominant component of the measured field is the direct antenna field and not the multipath. In addition, since the fields are strongest, there the highest signal-to-noise ratio is achieved for a given input power. The rectangular cuboid probed area S is chosen to be as small as possible so as not to increase the number of sampled points $N_i (i = x, y, \text{and } z)$, and consequently measurement time. The measurement parameters used are shown in Table I.

The very-near-field measurements of the miniaturized low-VHF antenna were conducted in a small indoor space, as shown in Fig. 9. To avoid unwanted EM coupling effects between the radiating element and the surrounding objects, the antenna is placed away from nearby objects, so that the scatterers are not within the antenna near-field reactive region. The RF field probe system consists of a fiber-coupled

TABLE I
MEASUREMENT PARAMETERS

Freq. (MHz)	d_p (mm)	Δs (mm)	N_i (i=x,y,z)	Probed area (cm × cm)
40	15 30 (Back)	5	N_x: 30 N_y: 27 N_z: 37	Top & Bottom: 13×14.5 Front & Back: 13×18 Left & Right: 14.5×18

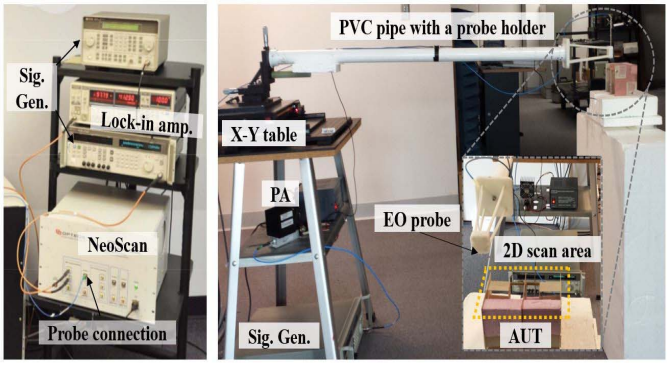

Fig. 9. Actual measurement setup for very-near-field measurements of the AUT. The measurements were performed in a small indoor space.

EO probe, PA, signal generators, lock-in amplifier, and NeoScan, including EO modulators and demodulators and sensitive RF components. The system is also equipped with a high precision two axes motor controlled X–Y table, which can move across an area of up to 25.4 cm × 25.4 cm, to position and move the probe. In this experiment,the EO probe is mounted via a lightweight PVC pipe connected to the X–Y table. The pipe provides a separation between all the supporting instruments and the AUT, as shown in Fig. 9. The surfaces of the rectangular box enclosing the AUT are scanned separately and the measured data are utilized for far-field prediction from postprocessing.

The raw data from the scan are multiplied by the calculated calibration coefficient α to obtain the absolute value of the tangential electric fields. Figs. 10 and 11 show the simulated and measured two-dimensional magnitude and phase distributions of the tangential electric field on the front, left, and top faces of the rectangular box. To compare the absolute value of the measured field with simulations, the available input power to the AUT delivered by the RF source employed for measurements is used to calculate the voltage at the antenna input terminals. The comparison between the measurement and simulation of near fields shows an excellent agreement between the magnitude of the measured and simulated results. Note that here the data comparison is absolute and not relative. There is a constant 30° phase difference between the measured and simulated results. The reason for this is that NeoScan system cannot measure the absolute phase, as the phase of the local oscillator in the system cannot be determined. Such a difference, however, does not affect the accuracy in the far-field characterization of the AUT, since the relative phase distribution is important. It should also be noted that the absolute phase for each surface is adjusted to that of an adjacent surface by making sure the measured values at one common edge agree.

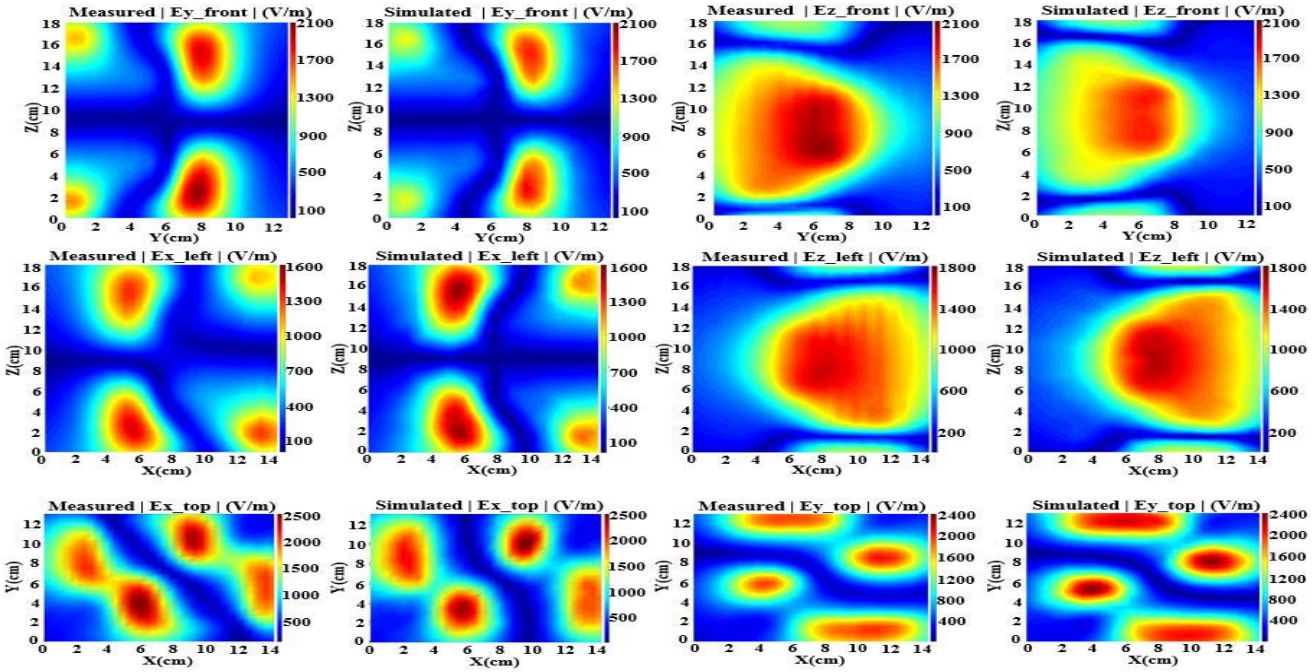

Fig. 10. Simulated (40.01 MHz) and measured (40.06 MHz) very-near-field maps showing the tangential components (magnitudes) of the electric fields on the front, left, and top surface of the imaginary box shown in Fig. 2.

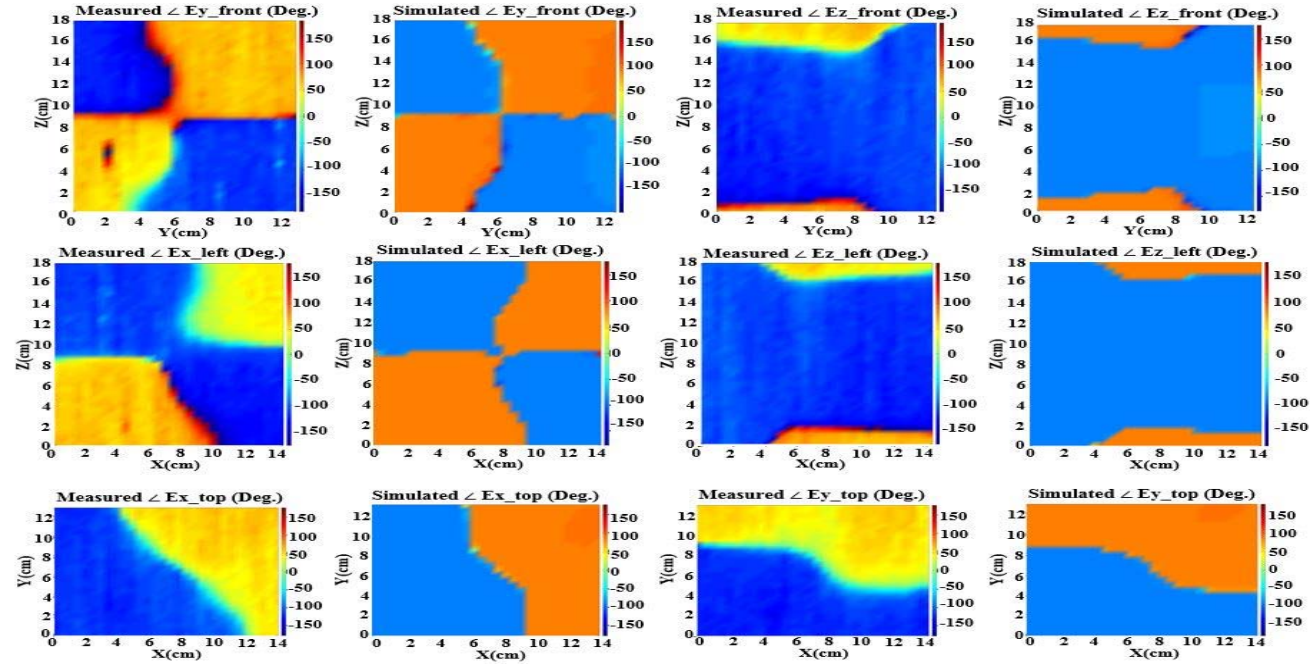

Fig. 11. Simulated (40.01 MHz) and measured (40.06 MHz) very-near-field maps showing the tangential components (phases) of the electric fields on the front, left, and top surface of the imaginary box shown in Fig. 2.

With this data, the far-field pattern and gain are evaluated using the procedure outlined in Section III. Fig. 12 shows the far-field radiation patterns in two orthogonal principal planes (E-plane and H-plane), together with simulated and measured results taken from the far-field measurements in the elevated range (using a small source module for feeding the AUT) discussed earlier. The patterns also closely resemble that of a short electric dipole with the maximum gain occurring at $\theta = 900^{\circ}$. It should be mentioned that the difference of the radiation pattern is mainly due to a small difference in the antenna feed configurations in the simulation and the actual setup. In the actual setup for the very-near-field measurement, a coaxial cable was connected for feeding the AUT. The antenna excites a current over the surface of the outer layer of the coaxial feed line, which in turn changes the near field on the surface of the scanned area adjacent to the coaxial feed.

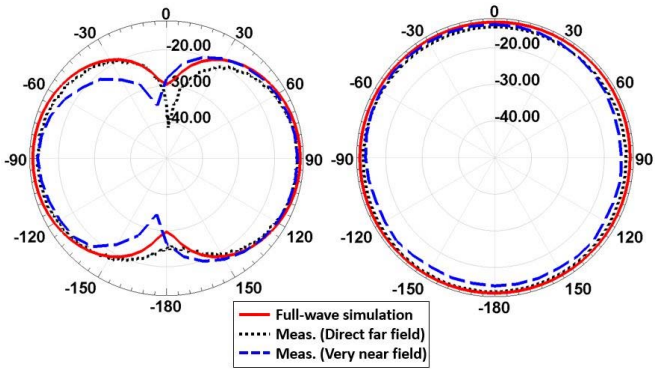

Fig. 12. Antenna radiation patterns (vertical polarization) in (a) E-plane (xz plane) and (b) H-plane (xy plane), computed by different approaches (the scale in the plot is ranging from -50 to -10 dB).

TABLE II
ANTENNA GAIN COMPARISON

Process	Simulation	Direct-far-field	Very-near-field
Center freq.	40.01 MHz	40.00 MHz	40.06 MHz
Peak gain	-12.8 dBi	-13.3 dBi	-13.6 dBi

This undesired effect can be eliminated by using a small source module, as reported in [2]. Table II presents a comparison of the antenna gain at resonance obtained from the proposed very-near-field method, simulation, and the elevated range far-field method.

V. CONCLUSION

A novel near-field measurement method for the characterization of 3-D radiation pattern and gain of antennas is presented. The approach is based on measuring the tangential components of electric field over arbitrary closed surfaces that enclose the AUT very close to the antenna boundary using a very small nonintrusive, all-dielectric, and broadband EO probe. This approach is shown to be a very effective and time-efficient method for accurate characterization of HF/VHF antennas for which anechoic chambers cannot be built and the far-field methods cannot provide accurate results due to different factors, such as the presence of the ground plane and proximity of feeding cables and measurement instruments. A new formulation based on the field equivalence principle and reaction theorem is developed to perform the near-field to far-field transformation without any approximations. To examine the validity of the proposed approach, an electrically small VHF (40 MHz) antenna is used. The measurements are performed indoor in a laboratory setting with objects removed from the near-field region of the antenna. The gain and radiation pattern are compared with simulation results and an elevated far field measured results, and excellent agreement is demonstrated.

REFERENCES

[1] *IEEE Standard Test Procedures for Antennas*, ANSI/IEEE Standard 149-1979, 1979.

[2] J. Choi, F. T. Dagefu, B. M. Sadler, and K. Sarabandi, "Electrically small folded dipole antenna for HF and low-VHF bands," *IEEE Antennas Wireless Propag. Lett.*, vol. 15, pp. 718–721, Mar. 2016.

[3] R. Azadegan and K. Sarabandi, "A novel approach for miniaturization of slot antennas," *IEEE Trans. Antennas Propag.*, vol. 51, no. 3, pp. 421–429, Mar. 2003.

[4] L. Mattioni and G. Marrocco, "Design of a broadband HF antenna for multimode naval communications," *IEEE Antennas Wireless Propag. Lett.*, vol. 4, pp. 179–182, 2005.

[5] G. Virone *et al.*, "Antenna pattern verification system based on a micro unmanned aerial vehicle (UAV)," *IEEE Antennas Wireless Propag. Lett.*, vol. 13, pp. 169–172, 2014.

[6] G. E. Barker, "Measurement of the radiation patterns of full-scale HF and VHF antennas," *IEEE Trans. Antennas Propag.*, vol. 21, no. 4, pp. 538–544, Jul. 1973.

[7] G. Le Fur, L. Duchesne, L. Durand, A. Bellion, and D. Belot, "Feasibility of indoor spherical near field antenna measurement facility in VHF range," in *Proc. 15th Int. Symp. Antenna Technol. Appl. Electromagn. (ANTEM)*, Jun. 2012, pp. 1–7.

[8] S. Villers and A. Malhage, "VHF probes for antenna measurement in a near field range," in *Proc. IEEE Conf. Antenna Meas. Appl. (CAMA)*, Nov. 2014, pp. 1–4.

[9] D. Serafin *et al.*, "Spherical near-field facility for microwave coupling assessments in the 100 MHz–6 GHz frequency range," *IEEE Trans. Electromagn. Compat.*, vol. 40, no. 3, pp. 225–234, Aug. 1998.

[10] EMAG Technologies, Inc. [Online]. Available: http://www.emagtech.com

[11] E. Joy and G. Rodrigue, "Applications of probe-compensated near-field measurements," *IEEE Trans. Antennas Propag.*, vol. 26, no. 3, pp. 379–389, May 1978.

[12] J. Shi, M. A. Cracraft, K. P. Slattery, M. Yamaguchi, and R. E. DuBroff, "Calibration and compensation of near-field scan measurements," *IEEE Trans. Electromagn. Compat.*, vol. 47, no. 3, pp. 642–650, Aug. 2005.

[13] M. S. Narasimhan and S. Ravishankar, "Probe uncompensated near-field to far-field transformation for scanning over an arbitrary surface," *IEEE Trans. Antennas Propag.*, vol. 33, no. 4, pp. 467–472, Apr. 1985.

[14] A. Taaghol and T. K. Sarkar, "Near-field to near/far-field transformation for arbitrary near-field geometry, utilizing an equivalent magnetic current," *IEEE Trans. Electromagn. Compat.*, vol. 38, no. 3, pp. 536–542, Aug. 1996.

[15] J. Oh, J. Choi, F. T. Dagefu, and K. Sarabandi, "Extremely small two-element monopole antenna for HF band applications," *IEEE Trans. Antennas Propag.*, vol. 61, no. 6, pp. 2991–2999, Jun. 2013.

[16] A. Capozzoli *et al.*, "Dielectric field probes for very-near-field and compact-near-field antenna characterization [measurements corner]," *IEEE Antennas Propag. Mag.*, vol. 51, no. 5, pp. 118–125, Oct. 2009.

[17] T. Pfeifer, T. Loffler, H. G. Roskos, H. Kurz, M. Singer, and E. M. Biebl, "Electro-optic near-field mapping of planar resonators," *IEEE Trans. Antennas Propag.*, vol. 46, no. 2, pp. 284–291, Feb. 1998.

[18] F. T. Dagefu, J. Oh, and K. Sarabandi, "A sub-wavelength RF source tracking system for GPS-denied environments," *IEEE Trans. Antennas Propag.*, vol. 61, no. 4, pp. 2252–2262, Apr. 2013.

[19] F. T. Dagefu, J. Choi, M. Sheikhsofla, B. M. Sadler, and K. Sarabandi, "Performance assessment of lower VHF band for short-range communication and geolocation applications," *Radio Sci.*, vol. 50, no. 5, pp. 443–452, May 2015.

[20] F. T. Dagefu *et al.*, "Short-range low-VHF channel characterization in cluttered environments," *IEEE Trans. Antennas Propag.*, vol. 63, no. 6, pp. 2719–2727, Jun. 2015.

[21] D.-J. Lee, N.-W. Kang, J.-H. Choi, J. Kim, and J. F. Whitaker, "Recent advances in the design of electro-optic sensors for minimally destructive microwave field probing," *Sensors*, vol. 11, no. 1, pp. 806–824, Jan. 2011.

[22] F. L. Pedrotti and L. S. Pedrotti, *Introduction to Optics*. Upper Saddle River, NJ, USA: Prentice-Hall, 1993.

[23] R. F. Harrington, *Time-Harmonic Electromagnetic Fields*. New York, NY, USA: Wiley, 2001.

[24] A. D. Yaghjian, "An overview of near-field antenna measurements," *IEEE Trans. Antennas Propag.*, vol. 34, no. 1, pp. 30–45, Jan. 1986.

[25] V. H. Rumsey, "Reaction concept in electromagnetic theory," *Phys. Rev.*, vol. 94, no. 6, p. 1483, Jun. 1954.

[26] S. C. Chapra and R. P. Canale, *Numerical Methods for Engineers*. New York, NY, USA: McGraw-Hill, 2012.

[27] C. A. Balanis, *Antenna Theory: Analysis and Design*. Hoboken, NJ, USA: Wiley, 2005.

[28] D.-J. Lee, J.-Y. Kwon, N.-W. Kang, and J. F. Whitaker, "Calibrated 100-dB-dynamic-range electro-optic probe for high-power microwave applications," *Opt. Exp.*, vol. 19, no. 15, pp. 14437–14450, Jul. 2011.
[29] M. L. Crawford, "Generation of standard EM fields using TEM transmission cells," *IEEE Trans. Electromagn. Compat.*, vol. EMC-16, no. 4, pp. 189–195, Nov. 1974.
[30] *Instruments for Industry*. [Online]. Available: http://www.ifi.com/images/stories/pdfs/TEM_Cells_IFI_CC_series.pdf
[31] A. V. Oppenheim and R. W. Schafer, *Digital Signal Processing*. Englewood Cliffs, NJ, USA: Prentice-Hall, 1975.

Kamal Sarabandi (S'87–M'90–SM'92–F'00) received the B.S. degree in electrical engineering from the Sharif University of Technology, Tehran, Iran, in 1980, double M.S. degrees in electrical engineering and mathematics, and the Ph.D. degree in electrical engineering from the University of Michigan, Ann Arbor, MI, USA, in 1989.

He was the Principal Investigator on many projects sponsored by the National Aeronautics and Space Administration, the Jet Propulsion Laboratory, the Army Research Office, the Office of Naval Research, the Army Research Laboratory, the National Science Foundation, the Defense Advanced Research Projects Agency, and a large number of industries. Currently, he is leading the Center for Microelectronics and Sensors funded in 2008 by the Army Research Laboratory under the Micro-Autonomous Systems and Technology Collaborative Technology Alliance program. He is also leading a newly established center in Microwave Sensor Technology funded by King Abdulaziz City for Science and Technology. He possesses 25 years of experience with wave propagation in random media, communication channel modeling, microwave sensors, and radar systems, and leads a large research group including two research scientists and 16 Ph.D. students. He is currently the Director of the Radiation Laboratory and the Rufus S. Teesdale Endowed Professor of Engineering with the Department of Electrical Engineering and Computer Science, University of Michigan. He has graduated 46 Ph.D. and supervised numerous post-doctoral students. He has authored many book chapters and over 250 papers in refereed journals on miniaturized and on-chip antennas, meta-materials, electromagnetic scattering, wireless channel modeling, random media modeling, microwave measurement techniques, radar calibration, inverse scattering problems, and microwave sensors. He has also had more than 580 papers and invited presentations in many national and international conferences and symposia on similar subjects. His current research interests include microwave and millimeter-wave radar remote sensing, meta-materials, electromagnetic wave propagation, and antenna miniaturization.

Dr. Sarabandi served as a member of the NASA Advisory Council from 2006 to 2010. He is a member of Commissions F and D of URSI and is serving as the Vice Chair of the USNC URSI Commission F. He was a recipient of the Henry Russel Award from the Regent of the University of Michigan, the GAAC Distinguished Lecturer Award from the German Federal Ministry for Education, Science, and Technology in 1999, the 1996 EECS Department Teaching Excellence Award, the 2004 College of Engineering Research Excellence Award, the IEEE GRSS Distinguished Achievement Award in 2005, the University of Michigan Faculty Recognition Award, the Best Paper Award at the 2006 Army Science Conference, the Humboldt Research Award from The Alexander von Humboldt Foundation of Germany in 2008, the Best Paper Award at the IEEE Geoscience and Remote Sensing Symposium, the 2010 Distinguished Faculty Achievement Award from the University of Michigan, the 2011 IEEE Judith A. Resnik Award by the IEEE Board of Directors, the 2013 Education Award by the IEEE GRSS, the Stephen S. Attwood Award from the College of Engineering, University of Michigan in 2016, and the Distinguished Alumni Award from the Sharif University of Technology. In the past several years, joint papers presented by his students at a number of international symposia (IEEE APS'95,'97,'00,'01,'03,'05,'06,'07,'16; IEEE IGARSS'99,'02,'07,'11,'14; IEEE IMS'01, USNC URSI'04,'05,'06,'10,'11, AMTA'06; URSI GA'08,'14; Eastern Snow Conference'16) have received best paper awards. He is listed in *American Men and Women of Science, Who's Who in America, and Who's Who in Science and Engineering*. He was an Associate Editor of the IEEE TRANSACTIONS ON ANTENNAS AND PROPAGATION and the IEEE Sensors Journal. Currently, he is serving as the President of the IEEE Geoscience and Remote Sensing Society and on the Editorial Board of the IEEE PROCEEDINGS.

Jihun Choi (S'12) received the B.S. degree in electrical engineering from Incheon National University, Incheon, South Korea, in 2010, and the M.S. degree in electrical engineering from the University of Michigan, Ann Arbor, MI, USA, in 2013, where he is currently pursuing the Ph.D. degree.

Since 2011, he has been with the Radiation Laboratory, Department of Electrical Engineering and Computer Science, University of Michigan, MI, USA, where he is currently a Graduate Research Assistant. His current research interests include antenna miniaturization, antenna measurement techniques, wave propagation modeling in highly cluttered environments, and low-power HF/VHF radio system design.

Ali Sabet received the M.Eng. degree in electrical engineering, and the M.Sc. and Ph.D. degrees in Physics from the University of Toronto, Toronto, ON, Canada, in 1993, 1996, and 2000, respectively.

In 2001, he joined the Cavendish Laboratory, Cambridge University, Cambridge, U.K., where he was involved in silicon microstrip sensors and high-energy particle-tracking instruments. In 2014, he joined EMAG Technologies Inc., Ann Arbor, MI, USA, where he has been involved in the development of the NeoScan, EMAG's turnkey electric field measurement system project, and is currently a Research Engineer.

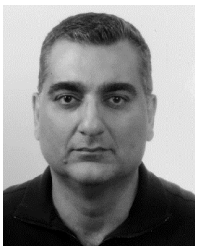

Kazem Sabet (S'88–M'95–SM'05) received the M.S. degree in electrical engineering from New York University, New York, NY, USA, in 1990, and the Ph.D. degree in electrical engineering from the University of Michigan, Ann Arbor, MI, USA, in 1995. His Ph.D. research involved computational modeling of planar circuits and antennas for microwave, and millimeter-wave applications.

He joined the Radiation Laboratory, University of Michigan, Ann Arbor, MI, USA. Since 1994, he has been served as the President of EMAG Technologies Inc., Ann Arbor, MI, USA. He has served as the Principal Investigator of more than 100 and industry funded research and development projects related to antennas, phased arrays, RF measurements, modeling, and simulation. He has also technically managed the development of several EDA and electromagnetic simulation software tools such as EM.Cube and RF.Spice A/D as well as NeoScan, EMAG's turnkey electric field measurement system. He holds eight U.S. patents in the field of planar antennas and phased arrays.

Dr. Sabet is a Senior Member of the Optical Society of America and SPIE. He was a recipient of the 1999 IEEE Marconi Award in Electronics and Communications.